Corrosion Science 63 (2012) 59–70

Contents lists available at SciVerse ScienceDirect

Corrosion Science

journal homepage: www.elsevier.com/locate/corsci

The effect of aluminium alloy secondary phases on aniline-based silane protection capacity

Monica Trueba [a,*], Stefano P. Trasatti [a], Daniel O. Flamini [b]

[a] Department of Physical Chemistry and Electrochemistry, Università degli Studi di Milano, Via Golgi 19, Milan 20133, Italy
[b] Department of Chemical Engineering, Universidad Nacional del Sur, Av. Alem 1253, Bahia Blanca 8000, Argentina

ARTICLE INFO

Article history:
Received 7 February 2012
Accepted 26 May 2012
Available online 9 June 2012

Keywords:
A. Aluminium alloy
A. Polymer coatings
C. Corrosion
C. Inhibition

ABSTRACT

Commercial wrought Al alloys with high content of intermetallic phases, namely, AA5083-H111, AA2024-T3 and AA7075-T6, were treated with N-(3-trimethoxysilylpropyl) aniline (AnSi) by a simple procedure. Characterization studies and corrosion experiments indicate that the hybrid film protection capacity is related in a complex way to the macromolecular network structure linked to the Al substrate composition. Nevertheless, barrier protection enhanced by a buffer effect and galvanic coupling, as aided by aniline units within the hybrid film, is indicated mostly. Results overall demonstrate synergistic effect against Al alloy corrosion by combining at a molecular level monomers of conducting polymers and silane functionalities.

1. Introduction

Conducting polymers (CP) constitute attractive materials for corrosion protection of metals [1,2]. The main properties that distinguish CP from organic molecules are their ability to conduct electricity and to bind/expel molecules or ions in response to an electrochemical potential. The complicated outcome of these concurrent phenomena as linked to corrosion processes is manifested by the on-going debate about CP protection mechanism(s), in particular for Al alloys. Galvanic coupling between metal and CP has been pointed out for ensuring effective corrosion inhibition [3–11]. The complexity of CP/Al alloy systems in corrosion science is also demonstrated by interrelated fundamental and practical limitations with a common factor - the use of contiguous CP films. Besides low processability and poor adhesion to active metals, the protection capacity of CP is strongly influenced by nature and surface preparation of the metallic substrate, CP properties, method of deposition, corrosion test and aggressive conditions used in performance assessment, etc. [11–15]. In our recent work, dealing with polypyrrole (PPy) electro-deposited on different Al alloys, the role of the rate at which structural and conformational changes are driven within the polymer network is also highlighted [11]. The inherent porosity at a molecular level can be overcome by using dopant ions with inhibiting properties, which are released during corrosion-induced CP reduction, but this approach fails in the presence of large defects [8,16,17]. Consequently, research activity increasingly aims at developing coatings constituted by an insulating matrix where CP clusters are distributed like (nano)composite formulations [10,18], multilayers [19] and copolymerization [20]. Iron-based alloys and polyaniline (Pani) are still the most investigated systems due to practical considerations, while less work has been devoted to Pani derivatives [21], in particular to those properly functionalized for direct surface modification [22]. To our knowledge, no studies on direct surface treatment of reactive metals with CP-functionalized silanes have been reported before our previous works with pyrrole-based silane [23] and aniline-based silane [24]. A recent study of composite sol–gel/PAni coating on AA2024 shows outstanding protection [25]. However, the thickness of silane sol–gel coatings (or multilayers/composites in general) is considerably higher than for chemical surface conversion coatings [26] or other pre-treatments such as silane-based [27,28].

The direct-to metal surface treatment with pyrrole-based silane (PySi) in the corrosion protection of Al alloys [23] showed that hybrid films with thicknesses of the order of microns can be obtained by simple immersion in the PySi hydrolysed solution and subsequent curing. The outstanding performance was attributed to the synergistic effect against metal degradation in terms of improved adhesion, high compactness and barrier/active actions as a result of pyrrole and siloxane homo-functional linking in a single macromolecular network, as promoted in the PySi solution. More recently, an aniline-based silane, namely, N-(3-trimethoxysilylpropyl)aniline (AnSi) (Fig. 1a), was investigated for corrosion inhibition of 1050-H24 Al alloy (AA) [24]. As obtained for PySi-based films, characterization studies indicated that PAnSi hybrid macro-network building on the metallic substrate is governed by the structure of AnSi soluble hybrid oligomers, being mainly composed by propyl-tethered siloxane chains and aniline N–H···N associates. The

* Corresponding author. Tel.: +39 0250314207; fax: +39 0250314300.
E-mail address: monica.trueba@unimi.it (M. Trueba).

0010-938X/$ - see front matter © 2012 Elsevier Ltd. All rights reserved.
http://dx.doi.org/10.1016/j.corsci.2012.05.028

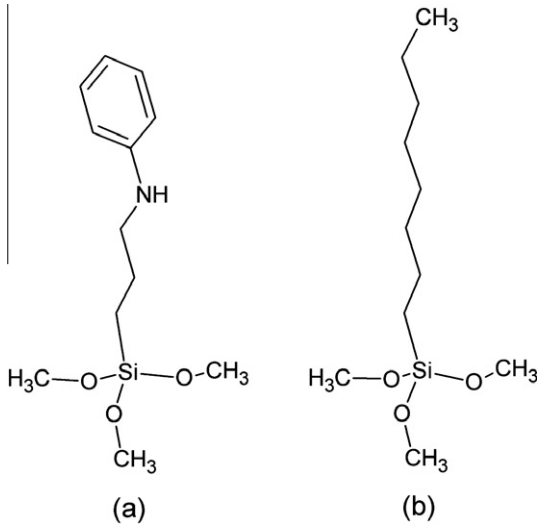

Fig. 1. (a) N-(3-trimethoxysilylpropyl)aniline (AnSi); (b) n-octyltrimethoxysilane (OcSi).

intermolecular homo-functional oligomerization of AnSi molecules was recently confirmed by liquid NMR (Supplementary data S1). The good performance against AA1050 corrosion was not only due to the improved adhesion and the high compactness, resulting from silanol adsorption/condensation at the metal surface and from three-dimensional PAnSi cross-linking. Aniline moieties act likely on demand for metal passivity recovery as barrier protection fails and/or permeability increases. To gain deeper knowledge of the protection potentialities of AnSi treatment, commercial wrought Al alloys with different composition, namely, AA5083-H111, AA2024-T3 and AA7075-T6, were investigated. Specimens modified by a simple procedure, i.e., immersion in a given AnSi solution and curing, were characterized by surface spectroscopic techniques. Protection performance evaluation was carried out by different corrosion experiments in near neutral NaCl 0.6 M solution. Alloys treated with octylsilane (Fig 1b) were also studied as a reference coating system.

2. Experimental part

2.1. Surface treatment and coating characterization

Surface modification was carried out on as-received commercial wrought Al alloys AA2024-T3, AA5083-H111 and AA7075-T6, as supplied by Aviometal Spa (Table 1). Pre-treatment with the aniline-based silane (AnSi) solution was performed as reported previously [24]. Briefly, Al substrates were cleaned with hexane, acetone and methanol in an ultrasonic bath, 15 min. each, and pre-heated at 130 °C for 20 min. in an open-to-air sand oven. Hot specimens were then immersed for 3 min. in a given AnSi solution, dried in a stream of hot air and thermally treated for one hour at the above reported pre-heating conditions. AnSi solutions were prepared at 4% v/v in a mixture of methanol/H_2O (95:5), pH 4.6 as adjusted with acetic acid, and left under stagnant conditions for 3 or 10 days at room temperature. The pH of the solutions did not change with time, as measured prior to their use, and pink coloration was clearly observed in the 10-days aged solution due to promoted N–H···N association in-between AnSi molecules [24]. Coated substrates prepared with 3- and 10-days aged AnSi solutions are denoted as PAnSi-3/AAxxx and PAnSi-10/AAxxx, respectively. The above-mentioned procedure was also used to prepare Al substrates modified with a 3-days aged octylsilane (OcSi) solution. Samples are denoted as POcSi-3/AAxxx.

Table 1
Chemical composition (wt.%) of commercial wrought Al alloys (Aviometal Spa).

Al alloys	Si	Fe	Cu	Mn	Mg	Zn	Ti	Cr
AA5083-H111	0.17	0.32	0.04	0.62	4.32	0.03	0.02	0.07
AA2024-T3	0.15	0.25	4.67	0.63	1.34	0.02	0.06	0.01
AA7075-T6	0.08	0.13	1.60	0.02	2.52	5.90	0.04	0.19

The structure/composition of PAnSi films on the Al alloys was investigated by Reflection–Absorption IR (RAIR) and X-ray Photoelectron (XPS) Spectroscopies. RAIR spectra were obtained with a Spectrum One (Perkin-Elmer) spectrophotometer in the range 4000–400 cm^{-1} (64 scans) with a spectral resolution of 4 cm^{-1} and equipped with a VeeMAX II accessory that allows changing the angle of incidence. For each coated alloy, three different incidence angles were used, 30°, 45° and 75°. An ESCA system (XI ASCII Surface Science Instruments) operating at 10^{-8}–10^{-9} torr with Al anode (1486.6 eV) and 1 eV of energy resolution was used to collect XPS spectra.

2.2. Corrosion experiments

Protection of the bare and silane-treated alloys was evaluated at room temperature in quiescent, naturally aerated, near neutral (pH 6.5 ± 0.2) 0.6 M NaCl solution, prepared with reagent grade NaCl (98%, Aldrich) and milliQ water.

Electrochemical corrosion experiments consisted in potentiodynamic polarization, potestiostatic measurements and free corrosion potential monitoring. Single-cycle anodic polarization curves were recorded at 10 mV/min after 10-min. equilibration at open circuit potential (OCP). As the forward current attained the preselected limiting value of 5 mA/cm^2, the direction of the scan was reversed, ending the measurement as the current became cathodic. In the cathodic polarization, only the forward scan was recorded at the same scan rate up to the current of −5 mA/cm^2. Potentiostatic experiments consisted in monitoring for 15 h the current during polarization at the pitting potential of the bare alloys, whose value was previously determined as described elsewhere [29]. Free corrosion potential as a function of time was measured by recording the OCP during 15 h. The electrochemical system consisted in a single-compartment O-ring cell with a working (active) surface of 1 cm^2, a Pt spiral counter electrode, and an external SCE as a reference, connected to the working compartment via a salt bridge containing the test solution and a Haber-Luggin capillary. Data were recorded by means of a PC driven PAR Model 273A using a SoftCorr™ II software.

Long-term immersion tests were performed according to the ASTM procedure G31 [30]. Bare and coated specimens, whose edges were masked with adhesive tape, were positioned vertically in cylindrical vessels containing test NaCl solution. Exposure continued 30 days at 30 °C under naturally aerated conditions.

The morphology of corroded specimens was examined using a LEO 1430 scanning electron microscope (SEM) equipped with an EDX spectrometer at a chamber pressure of 8×10^{-6} torr and 20 keV accelerating voltage. Cross-section specimens were embedded in a cold-working resin and then polished up to 1 μm with diamond paste in non-aqueous solvent.

3. Results and discussion

3.1. Coating characterization

Several common features were obtained with PAnSi-coated AA1050 [24]. All AnSi-treated alloys kept a bright-metallic look due to formation of uniform transparent films. Slight-brownish coloration was visually noticed after treatment with AnSi-10

solution (pink). The estimation of film thickness by SEM was not possible because a metal/film interface was not distinguishable. RAIR spectra of PAnSi-3 and PAnSi-10 coated alloys showed no differences, even those of PAnSi-coated AA2024 with distinct spectral features. The structure of PAnSi coatings is mainly characterized by intermolecular siloxane linkages (silanol group condensation) and N–H···N associates. In XPS analysis, the main lines of all PAnSi-coated alloys were O1s, C1s, N1s and Si2p, with the exception of PAnSi-10/AA7075 for which a 3.3 at.% of Mg was found. The features of the O1s and Si2p lines deconvolution resembled closely those obtained for PAnSi/AA1050, whereas important differences were obtained in the high resolution analysis of the C1s and N1s lines. The peaks of C–N species and of O=C–O were positioned at higher binding energies as AnSi-3 solution was used for surface modification, more notable for AA2024 substrate. Information about the effect of Al alloy secondary phases on the hybrid coating composition was obtained from N1s line deconvolution. The structure of POcSi/AAxxx does not depend on the Al alloy nature, and the films thicknesses are between 2–5 μm (Supplementary data S2). On these bases, the RAIR spectra of PAnSi-3/AA2024 and the XPS N1s line analysis of AnSi-treated alloys are presented and discussed in what follows.

3.1.1. RAIR characteristics of PAnSi-3/AA2024

Fig. 2 compares the RAIR spectra of all PAnSi-3 coated specimens at the incidence angles of 45° (top) and 75° (bottom).The spectral features of PAnSi-3/AA2024 (Fig. 2b) are notably different from those of coated AA5083 and AA7075. Since the AnSi solution presented the same characteristics, such spectral "distortion" is attributed to the interaction between Cu-rich intermetallic particles and aniline moieties upon surface modification. The significant broadening of the NH stretching region (3550–3000 cm^{-1}) not only reveals the presence of NH^+ species (~3370 cm^{-1}) [31], but it also results from C=N stretches and C=C stretches overtone/combination (shoulder at 3200 cm^{-1}) [32]. The low frequency region shows a strong contribution of quinoid structures due to characteristic vibrations at ~1660, 1575, 1515 and 800–830 cm^{-1}(–C=C–C=N–, C=C and C=N stretching, and C–H deformation, respectively) [32–34]. The intensity of the stretching vibrations increases with respect to that of the typical bands of benzenoid structures (~1600, 1500, 750 and 695 cm^{-1}) [24] at higher incidence angle (75°). In addition, at both incidence angles, the bands corresponding to C–N stretching are very weak (1320–1250 cm^{-1}). All these features indicate the presence of oxidized N-substituted aniline oligomers such as emeraldine salt (EMS) and/or pernigraniline (PN) [35], promoted by Cu^{2+} release from the alloy surface with subsequent reaction with aniline to produce Cu^+-aniline complexes. Although Cu(I)-π electrostatic and specific orbital interactions are particularly enhanced in N-substituted anilines [36,37], coordinative bonding between Cu and N involving vacant d orbitals and electron lone pair, respectively, is also feasible.

3.1.2. X-ray photoelectron spectroscopy

XPS high resolution analysis of N1s line for PanSi-3 and PanSi-10 films on Al alloys is summarized in Table 2 [38,39]. Both PAnSi-coated AA5083 substrates show a single N^+ peak at about 400 eV pointing out an important contribution of N–H···N aggregates. Conversely, two N^+ peaks characterize PAnSi/AA2024 specimens with the higher energy peak being attributed to charge-deficient imine-like nitrogen (=N^+- ⩾ 60%). A non-negligible amount of the latter species (40%) is also obtained for PAnSi-3 on Zn-rich AA7075, but N–H···N structures prevails with AnSi-10 solution (PAnSi-10/AA7075).The variable nitrogen species in the hybrid PAnSi films indicate that each metallic surface reacts in a specific way upon immersion in the corresponding AnSi solution due to Al alloy secondary phase effect. In the case of AA2024, the

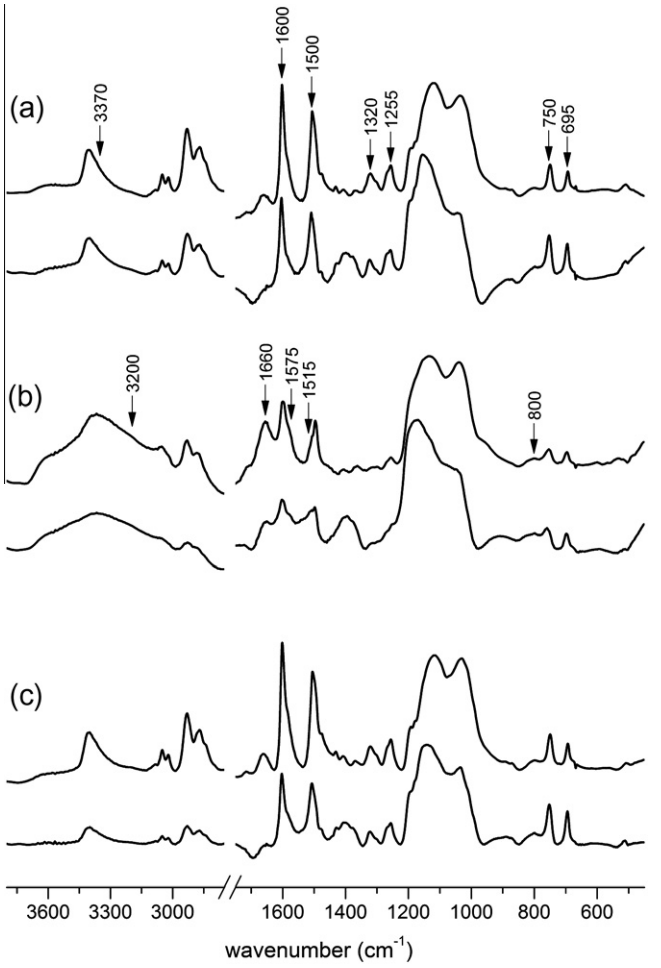

Fig. 2. RAIR spectra at 45° (top) and 75° (bottom) of PAnSi-3 coated Al alloys: (a) AA5083; (b) AA2024; (c) AA7075.

prevailing =N^+- species point to the presence of EMS and/or PN units, in good agreement with RAIR results (Fig. 2b). The importance of Cu(I)-π(N) interactions is confirmed by the composition of PAnSi-3 and PAnSi-10 films being almost independent of AnSi solution aging time. The opposite behavior of PAnSi-coated AA7075 suggests that possible interactions between Zn and aniline functionalities [40] are hindered due to enhanced dissolution of $MgZn_2$ upon treatment with AnSi-10 solution [41]. Actually, the survey spectrum of PAnSi-10/AA7075 revealed 3.3 at.% of Mg on the surface, indicating important Mg incorporation into the hybrid network, more probably as oxo-complexes according to the high acetate content obtained in the C1s line (~289 eV). Mg reactivity could also influence the lower content of =N^+- species in PASi-3/AA7075 as compared to PAnSi-3/AA2024. However, besides well-documented Cu(I)-π(N) strong interactions [36,37], dealloying of Al_2CuMg inclusions (S phase) in AA2024 producing Cu-rich remnants [42], in addition to the lower ionization energy of Cu [43] and the higher mobility of Cu^+ ions, converge to favor Cu-aniline moiety interactions. Interestingly, no Mg was detected on PAnSi-coated AA5083 (Mg-rich Al alloy), which suggests distinct siloxane bonding due to the chemical reactivity of the Mg_2Si phase [44]. The dealloying of this intermetallic produces surface silicon-enrichment, thus promoting formation of $Si_{(metal)}$–O–$Si_{(film)}$ linkages with concomitant suppression of Mg leaching and formation of $Mg(OH)_2$ and/or Mg-aniline oxo-complexes at the metal/film interface. These processes would be more favored if AnSi-10 solution is used in AA5083 surface modification.

Table 2
XPS binding energies (eV), linewidths (eV) and intensities (%) of the N species derived from N1s line analysis of PAnSi-3 and PAnSi-10 films on Al alloys.

AA 5083		AA 2024		AA7075		Chemical assignment
PAnSi-3	PAnSi-10	PAnSi-3	PAnSi-10	PAnSi-3	PAnSi-10[a]	
399.8	399.7	400.3	399.6	399.6	400.3	$=NH^+$, $-N^{\bullet+}$
2.3	1.9	1.8	1.8	1.9	2.5	
100	100	34	41	60	100	
		402.1	401.1	401.4		$=N^+-$
		2.0	1.8	2.0		
		67	60	40		

[a] 3.3 at.% of Mg in the survey XPS spectrum.

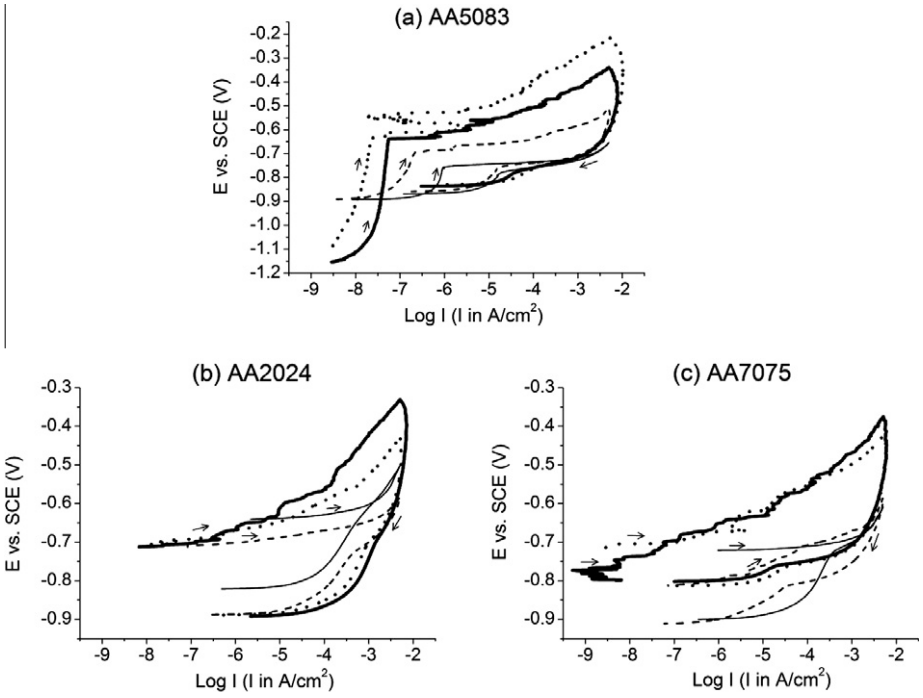

Fig. 3. Single-cycle anodic polarization (10 mV/min) of bare and silane-treated Al alloys in near-neutral naturally aerated 0.6 M NaCl: (—) bare alloy; (▬) PAnSi-3; (•••) PAnSi-10; (---) POcSi-3.

On these bases, metal-π(N) complexes are favored in the presence of Cu and Zn as in AA2024 and AA7075 substrates. Conversely, oxo-metallized complexes of weaker nature are more likely with Mg, as indicated by the composition of PAnSi-10/AA7075 and PAnSi-coated AA5083. These results allow to propose that the $=N^+-$ contribution of about 20% in PAnSi/AA1050 [24] is probably due to interaction of Fe-rich impurities with aniline moieties [39,45].

3.2. Protection against anodic dissolution

Single-cycle anodic polarization scans of bare and silane-treated alloys are shown in Fig. 3. PAnSi-coated substrates exhibit a more positive shift in the forward scan than that obtained with OcSi treatment, while no trend is observed in the reverse scans. Remarkable barrier-type action of PAnSi films on AA5083 (Fig. 3a) is manifested by a large passive region as the potential is shifted anodically. It is to be noticed that, contrary to AA1050 [24], POcSi-3 film on AA5083 provides some barrier protection as well, which supports strong siloxane bonding to the metallic surface promoted by silicon enrichment of the alloy surface (S2). Siloxane-defective metal/film interfaces are indicated for PAnSi-coated AA2024 and AA7075 with no current-independent potential region at the beginning of the scan. Nevertheless, this region begins at much lower current densities and, except for PAnSi-10/AA7075, at more negative potentials than those of bare alloys, which suggests an inhibiting action against cathodic processes at the corresponding buried interfaces. The different response of PAnSi-10/AA7075 could suggest an improved barrier action due to an Mg-rich hybrid film (Table 2). In the case of AA2024, similar behavior has been observed during anodic polarization in chloride solutions if treated with silanes containing small quantities of inhibitors such as tolyltriazole and benzotriazole [46], as well as if quinoline compounds are added to the test solution [47]. As a further argument, the role of the inhibitor structure on the corrosion of AA2024 and AA7075 alloys has been demonstrated recently [48].

Closer examination of forward scans in Fig. 3 reveals an apparent correlation between the magnitude of ennobling and the NH^+ contribution in the hybrid film composition (Table 2). Only for PAnSi films on AA1050 [24], neutral NH species ($\geqslant$50%) were detected on the surface and the most retarded breakdown was obtained during anodic polarization (e.g., in PAnSi/AA1050 shifted to about +600 mV with respect to bare alloy). The breakdown of PAnSi/AA5083 (Fig. 3a) is shifted only +200 mV (on average) with respect to the bare alloy, despite the significant barrier action. The corresponding PAnSi film surfaces are characterized by a single

NH^+ peak. If imine-like $=N^+$- species are also present, as in PAnSi-coated AA2024 and PAnSi-3/AA7075, no distinct breakdown is obtained (Fig. 3b and c). Accordingly, the performance of PAnSi coatings appears compromised by the contribution of charge deficient nitrogen species, promoted during film deposition. Such a trend is reasonably explained in terms of higher ionic conductivity and favored inward-migration of Cl^- ions to the metal/film interface. Despite this negative effect, metastable-like (macro)pitting [49] is indicated by sequences of rapid current rise and stabilization, more noticeable in PAnSi-coated AA2024 and AA7075. This strongly suggests that, under conditions of limited siloxane bonding at the metal/film interface and/or film degradation by corrosion, aniline moieties within the hybrid network favor metal passivity recovery. Similar "staircase" rise of current with potential was also observed with alloys treated with PySi owing to the repairing effect of PPy moieties in the hybrid film [23].

The performance of PAnSi films was evaluated also by polarization of the specimens at the pitting potential (E_{pit}) of bare alloys up to 15 h. E_{pit} was determined as reported elsewhere [29]. Fig. 4 shows the current–time responses of bare, PAnSi- and POcSi-coated AA5083. The response of bare alloy in the mA/cm^2 range is featured by decreasing currents during the first three hours (Fig. 4a), which indicates the formation of a protective corrosion layer probably due to surface enrichment with $Mg(OH)_2$ and $SiO_2{\cdot}nH_2O$ deposits [44]. Conversely, PAnSi-coated alloys show current stabilization at a values below 10 nA/cm^2 (Fig. 4b). Although the extent of localized attack was higher in PAnSi-3/AA5083, inhibition of the cathodic activity of Fe-rich particles, unconstrained by the size of intermetallic particles, was indicated by SEM (Fig. 5). Synergism in the protection mechanism due to Mg-rich metal/film interface acting as O_2 barrier and to PAnSi buffer effect on alkalinization at coating defects, is proposed for PAnSi/AA5083 system. The buffer effect can be reasonable explained by the combination of labile protons in N–H···N aggregates with OH^- ions produced near Fe-rich intermetallic particles [29]. The role of aniline moieties within the siloxane network is confirmed by the poor inhibition obtained with POcSi-3 film, as manifested by increasing negative currents with time (Fig. 4c). Differently from AA5083 substrates, no protection by PAnSi films is obtained for AA2024 and AA7075 substrates at the corresponding E_{pit} (Fig. 6). Also, suppression and arrest of corrosion due to deposition of oxide/salt products is indicated by the current–time response of bare alloys. The current rise in the coated

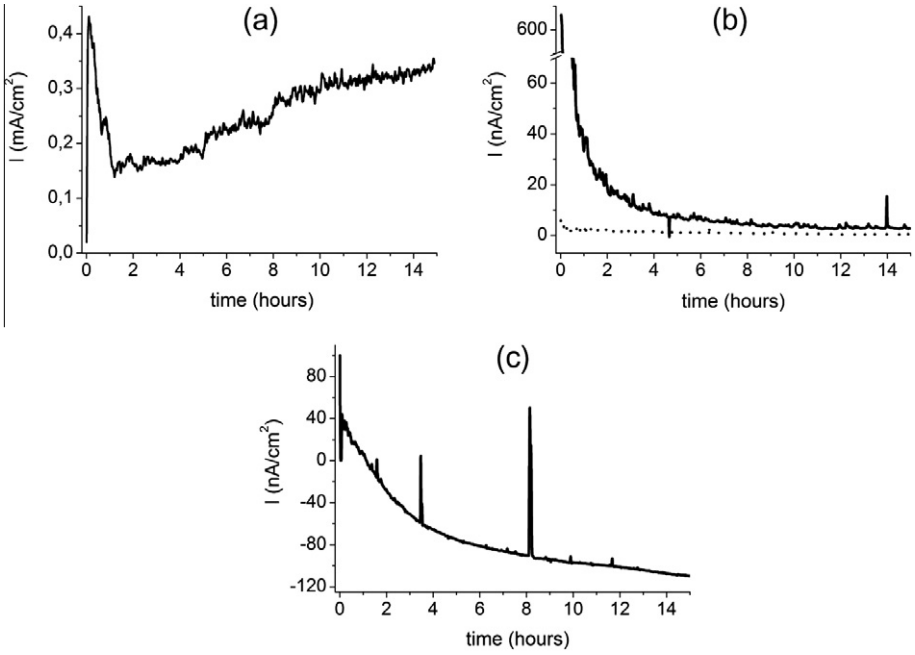

Fig. 4. Current response as a function of time of bare and silane-treated AA5083 during polarization at the pitting potential of bare alloy (E_{pit} = −740 mV vs. SCE) in naturally aerated near neutral 0.6 M NaCl solution: (a) bare alloy; (b) PAnSi-3(solid line) and PAnSi-10 (dotted line); (c) POcSi-3.

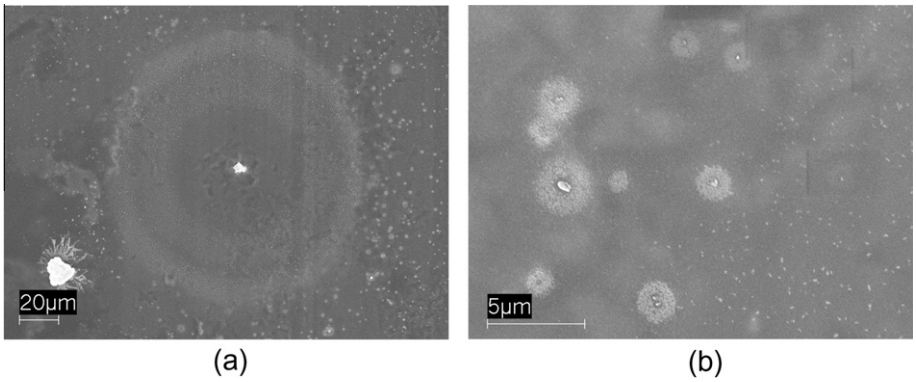

Fig. 5. Surface SEM images of PAnSi-10/AA5083 after polarization at the pitting potential of bare alloy in naturally aerated near neutral 0.6 M NaCl solution.

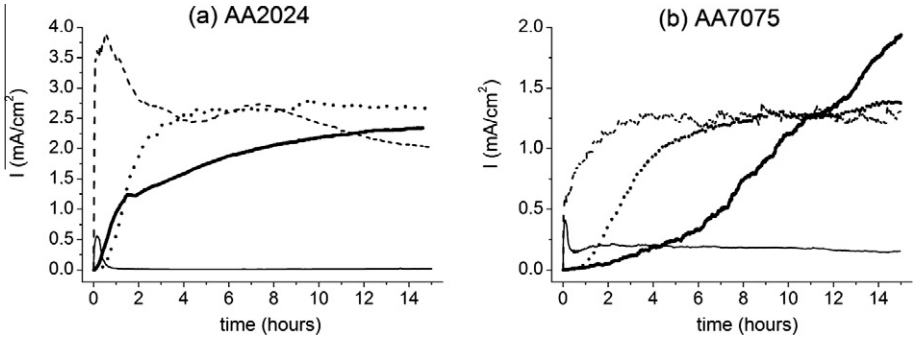

Fig. 6. Current response as a function of time of uncoated and silane-treated AA2024 and AA7075 during polarization at E_{pit} (vs. SCE) of the bare alloys: (a) −637 mV, (b) −715 mV; in naturally aerated near neutral 0.6 M NaCl solution: (—) bare alloy; (▬) PAnSi-3; (●●●) PAnSi-10; (- - -) POcSi-3.

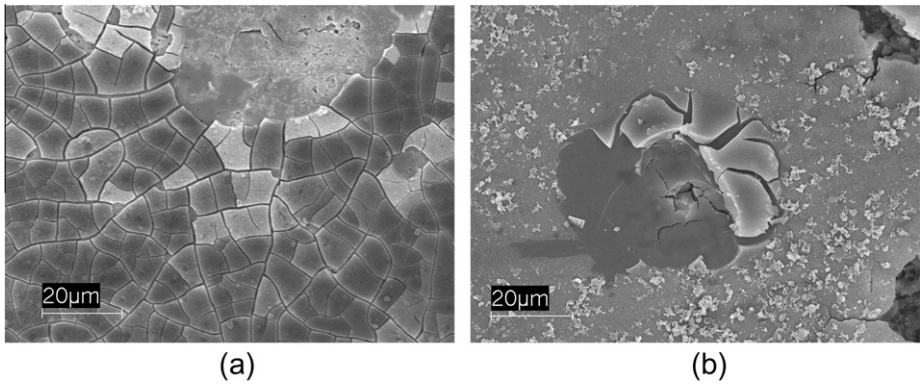

Fig. 7. Surface SEM images of (a) bare AA7075 and (b) PAnSi-3/AA7075 after polarization at the pitting potential of the bare alloy in naturally aerated near neutral 0.6 M NaCl solution.

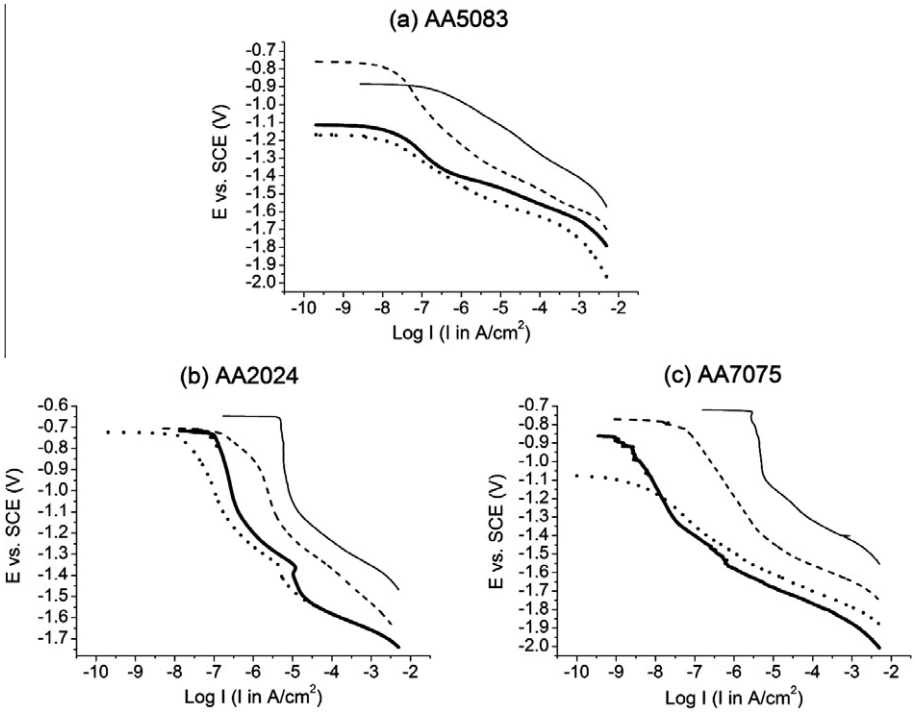

Fig. 8. Cathodic polarizations (10 mV/min) of bare and silane-treated Al alloys in near-neutral naturally aerated 0.6 M NaCl: (—) bare alloy; (▬) PAnSi-3; (●●●) PAnSi-10; (- - -) POcSi-3.

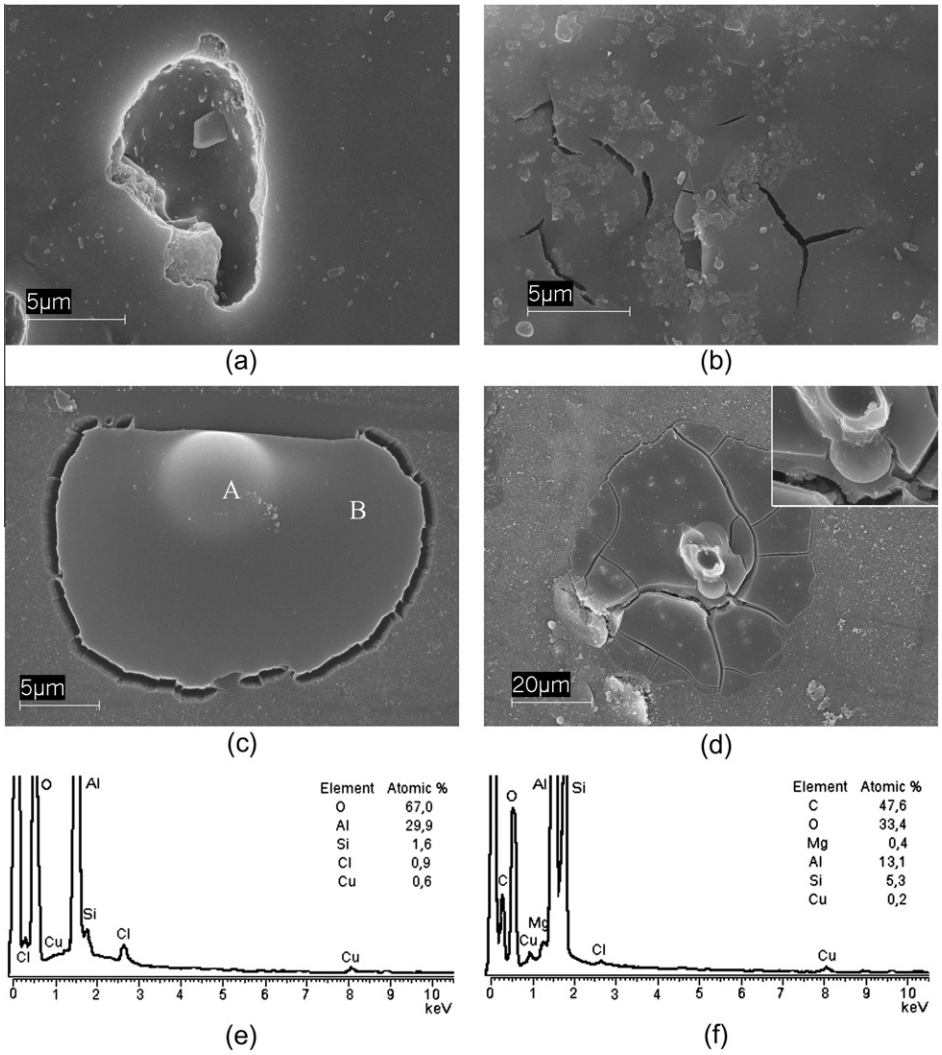

Fig. 9. Surface SEM examination of AnSi-treated Al alloys after cathodic polarization in 0.6 M NaCl: (a) PAnSi-3/AA5083; (b) PAnSi-10/AA5083; (c–f) PAnSi-3/AA2024, EDX spectra and elements composition in (e and f) correspond to sites A and B, respectively, in (d).

alloys suggests sub-surface crevice corrosion stimulated by defects at the metal/film interface [50], which promote hydrogen evolution and formation of corrosion products with consequent film rupture and disbondment. Differences in corrosion morphology between bare and PAnSi-coated substrates are clearly discernible for AA7075 in Fig. 7. Despite the negative result, current increases with time for both alloys in the following order: PAnSi-3 < PAnSi-10 < POcSi-3, pointing to improved protection by the hybrid network. Lower currents than AA2024 modified substrates for all coated AA7075 specimens indicate more stable metal/film interfaces. Doubts arise with respect to the inhibiting action of PAnSi by possible Cu- and Zn-aniline interactions. However, these can be hindered by growing Al hydr(oxide) products at E_{pit}, which is supported by the fact that Zn becomes anodic to Al in the presence of Al_2O_3. The results suggest that PAnSi-coated AA2024 and AA7075 needs be polarized to the active direction for effective protection. Accordingly, the "staircase" shape of the forward curves of single-cycle anodic polarization is related to metastable passivity impelled by aniline moieties re-oxidation during positive potential scan.

3.3. Protection against microgalvanic corrosion

Separate samples were submitted to cathodic polarization and electrochemical responses are shown in Fig. 8. Like for anodic polarization, AnSi-modified substrates show a higher shift of the curves, in this case towards lower cathodic currents, contrary to OcSi-treated alloys. Besides higher barrier action to oxygen and proton reduction, the change of the shape of the curves reflects different kinetic paths. PAnSi/AA5083 specimens, as well as PAnSi-10/AA7075 (containing Mg oxo-complexes in the hybrid network), are polarized at the beginning of the scan at ca. −1.1 V vs. SCE (Fig. 8a), which can be explained by the presence of Mg-rich precipitates [51] and/or Mg-aniline complexes at the buried interface [6]. However, with AA5083 substrates, a quite homogeneous metal/film interface is indicated by the closely similar potential of PAnSi-coated AA5083 at the beginning of the anodic polarization (ca. −1.1 V) (Fig. 3a). This further highlights the above-mentioned distinct siloxane covalent bonding due to Mg_2Si phase reactivity. Uniform metal/film interface is indicated also for PAnSi/AA2024 with potentials of −0.71 V vs. SCE (on average) at the beginning of both anodic and cathodic scans (Figs. 3b and 8b), despite siloxane-bonding limitations, due to Cu-aniline specific interactions. These probably account for the peak in the current density at very negative potentials (Fig. 8b) that indicates a change in the mechanism of the cathodic reactions associated with a conductive state transition due to galvanic coupling [4,6,7,24]. Conductive state transition is also suggested for PAnSi-3/AA7075 (Fig. 8c) though less defined presumably due to hindered and/or weaker coupling phenomena [10,40]. Another important

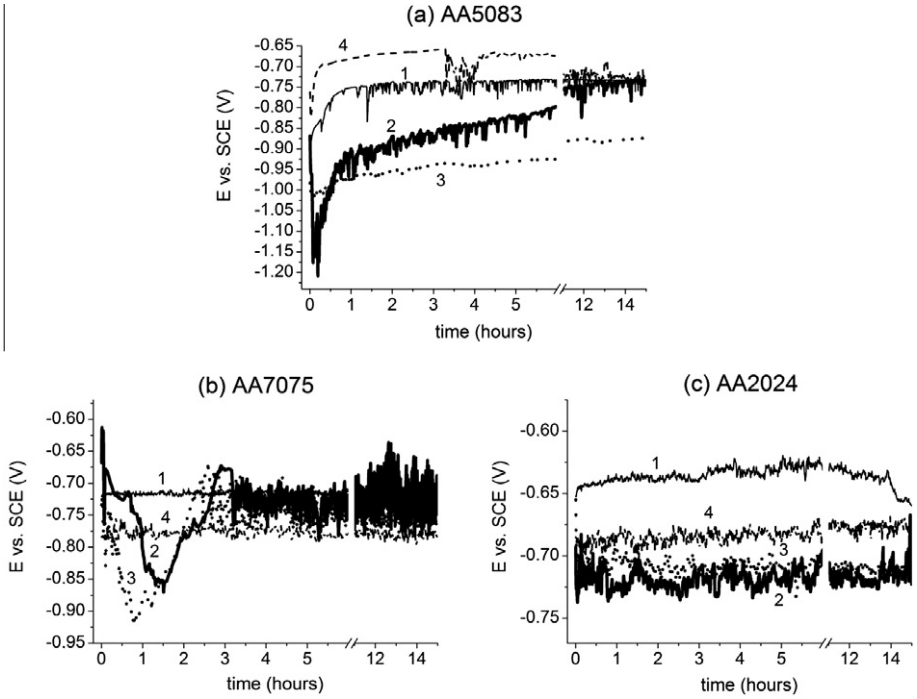

Fig. 10. Open-circuit potential response as a function of time of bare and silane-treated Al alloys in near-neutral naturally aerated 0.6 M NaCl: 1- bare (—); 2- PAnSi-3 (▬); 3- PAnSi-10 (●●●); 4- POcSi-3(- - -).

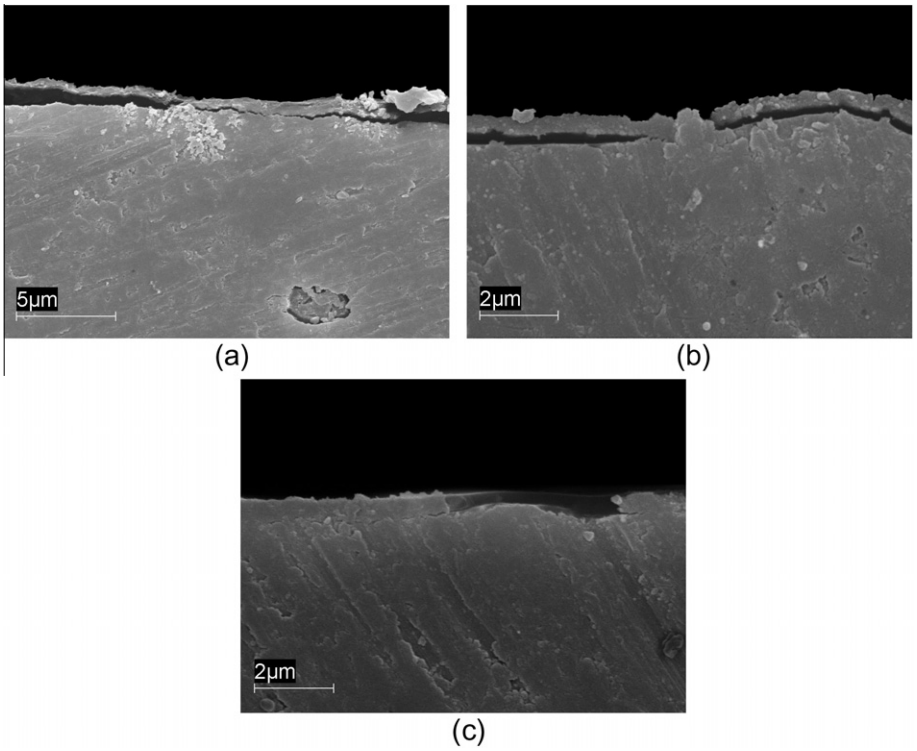

Fig. 11. Cross-section SEM images of AnSi-treated Al alloys after open-circuit potential monitoring in near-neutral naturally aerated 0.6 M NaCl: (a) PAnSi-3/AA5083; (b) PAnSi-3/AA7075; (c) PAnSi-10/AA2024.

observation regards the very negative potential at which cathodic peaks occur compared with contiguous polymer films (typically above −1 V) [4,6,7]. It can be argued that limited charge transfer reactions result from the non-conducting siloxane network in which aniline moieties are arranged as micro-conducting paths. Nevertheless, the cathodic peak position at a lower potential and current in PAnSi/AA2024 with respect to PAnSi/AA1050 [24], indicates a better interconnectivity in the former system due to Cu–π(N) complexes and/or aniline oxidized moieties (Table 2).

Surface SEM examination after cathodic polarization of PAnSi-10 coated specimens revealed film cracking and detachment with significant amount of undercoating corrosion products, indicating

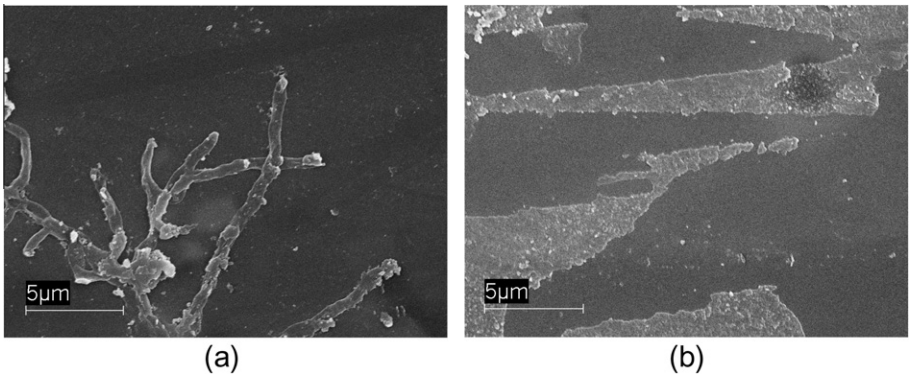

Fig. 12. Surface SEM images of AnSi-treated AA7075 after one-month immersion in naturally aerated near neutral 0.6 M NaCl: (a) PAnSi-3/AA7075; (b) PAnSi-10/AA7075.

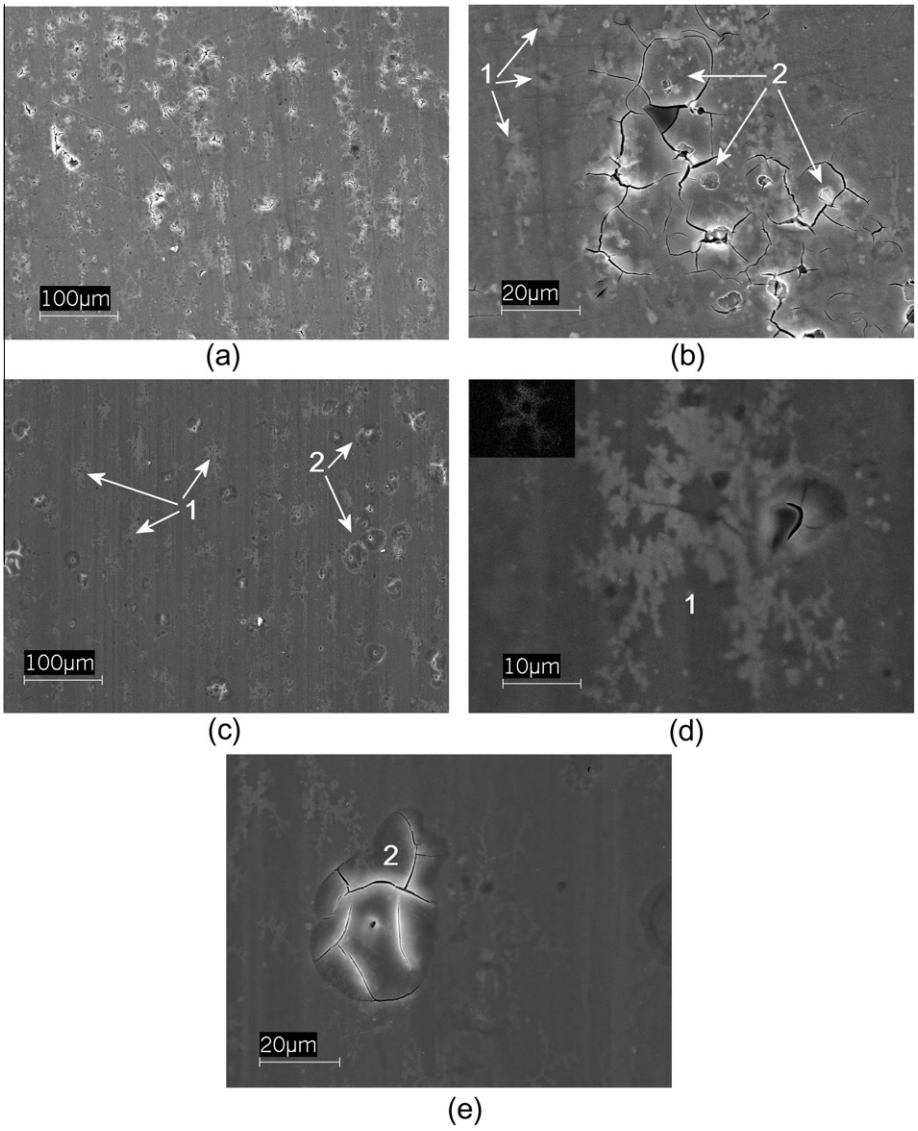

Fig. 13. Surface SEM images of PAnSi-coated AA2024 after one-month immersion in naturally aerated near neutral 0.6 M NaCl solution: (a and b) PAnSi-10/AA2024; (c–e) PAnSi-3/AA2024. Inset in (d): Cu Ka1 EDX map analysis. Arrows in (b and c) point two types of localized attack morphology: Cu-rich deposits (1) and pits (2).

higher proton mobility. This observation points to more permeable PAnSi-10 films due to the higher contribution of N–H···N aggregates since the growth of siloxane chains is simultaneously promoted by AnSi solution aging time (S1). Only for PAnSi/AA5083 system the amount of corroded surface was higher in PAnSi-3 coated alloy. Smooth nascent pit-like sites, reflecting decomposition of a well-adherent film rather than its rupture, were observed on less damaged regions (Fig. 9a and b). This result indicates that

improved overall protection of AA5083 by PAnSi-10 film results from a more stable Mg-rich metal/film interface, promoted during the surface treatment. In the case of PAnSi-3/AA2024, accumulation of spherical particles in a rounded, compact and apparently adherent film zone were systematically observed (Fig. 9c and d). Corrosion products on the film surface prevail only outside the circular cracks, indicating that degradation reactions are localized at the film/solution interface. EDX analysis indicated Al (hydr)oxi-chlorides and some copper on these sites (Fig. 9e and f). It was noticed no carbon but silicon increasing up to about 3.5 at.% in the well-developed particles (inset in Fig. 9d). These findings suggest that the buffer effect and the possible selective action of aniline moieties on Cl^- inward migration [52] are enhanced by Cu enrichment due to matrix dissolution near cathodic Al–Cu–Fe–Mn [42]. Thus, inhibition of such highly reactive sites by Cu-aniline galvanic coupling is more likely.

Open circuit potential (OCP) monitoring as a function of time (15 h) allowed to confirm different metal/film interface properties as determined by the AnSi solution and the nature of the Al alloy. The behavior of PAnSi/AA5083 specimens (Fig. 10a) gives evidence to the improved barrier action of the film obtained with AnSi-10 solution due to more stable Mg-rich metal/film interface. Cross-section SEM examinations revealed notable accumulation of corrosion products at the PAnSi-3/AA5083 interface (Fig. 11a), in agreement with progressive OCP oscillation with strong negative transients to values close to that of the bare alloy. In the case of AnSi-treated AA7075 substrates (Fig. 10b), OCP rapidly rises towards the rest potential of bare alloy with positive transients after about 12 h, being more marked in PAnSi-3/AA7075. The improved barrier action with time indicates the evolution of PAnSi/AA7075 system towards the galvanic coupling Zn–aniline with more favored O_2 reduction. SEM cross-section examinations revealed corrosion products mainly localized within the film (Fig. 11b). The apparent detachment of the coating, according to film profile matching that of the metallic substrate, points to an originally stressed interface due to transport-controlled degradation processes. Coupled state for an active repairing effect is also indicted for PAnSi/AA2024 specimens by the progressive shift of potential fluctuations to values close to that of bare alloy (Fig. 10c) [4]. Nevertheless, a more stable metal/film interface is indicated by OCP positive oscillations of about 100 mV, systematically below that of the bare alloy, over almost all the measurement time. Tightly bonded film with negligible alloy corrosion was observed at the end of the test (Fig. 11c). These results support the dislocation of cathodic oxygen reduction from the metal/film to film/solution interface, assisted by oxidized aniline moieties in the hybrid network.

The excellent protection of PAnSi films, in particular PAnSi-3, was definitely confirmed by examination of specimens submitted to uninterrupted immersion in 0.6 M NaCl solution for 30 days. No opacity due to oxide/salt precipitates was observed on PAnSi-coated AA5083 surfaces at naked eyes, contrary to bare and OcSi-treated alloys. In addition, PAnSi-3 coated AA2024 and AA7075 exhibited a bright, metallic-like, slight brownish appearance at the end of the test. SEM analysis of PAnSi-3/AA7075 showed filiform corrosion with very narrow filaments spreading out randomly from one or more initiation sites (Fig. 12a), indicating exceptionally good long-term stability under the present test conditions. Less effective PAnSi-10/AA7075 system was manifested by widespread blanket-like undercoating corrosion (Fig. 12b). A similar finding was obtained for PAnSi-10/AA2024 but with higher extent of local damage (Fig. 13a and b), featured by undercoating Cu-rich deposits (1) of irregular shape and pitting with film rupture (2). The two types of attack were also noticed on PAnSi-3/AA2024 (Fig. 13c) though with well-different morphology. Cu-rich deposits under the film exhibit dendritic look and the pits, surrounded by a darker well-adhered film zone were very small, as illustrated in Fig. 13d and e. The structured "extraction" of Cu from the alloy surface (1) suggests better interconnectivity of aniline moieties in the hybrid film with decrease of Al–Cu galvanic coupling. This mechanism was also proposed for spin-coated Pani [3] and electrodeposited PPy [11]. The morphology (2) resembles that obtained under more extreme conditions (Fig. 9c and d), with H^+ reduction as source of alkalinity during polarization to very negative potentials, but defects are in a passive state. Accordingly, under open circuit conditions, the re-oxidation of aniline moieties driven by cathodic oxygen reduction enhances the anodic galvanic protection of PAnSi films. This result supports previous observations on the role of oxygen in the galvanic coupling of CPs and AA2024 [7,16,18a].

4. Conclusions

As-received wrought Al alloys were modified with an aniline-based silane (AnSi) by a simple procedure. Very uniform thin films with transparent appearance were obtained. Characterization studies have revealed specific interactions with aniline moieties determined by Al alloy composition and/or surface treatment conditions. Metal–π(N) complexes are favored in the presence of Cu and Zn, while oxo-complexes of weaker nature are formed with Mg. The Al alloy corrosion is more retarded by hybrid PAnSi coatings than by a typical organosilane-based film such as POcSi, consistent with three-dimensional cross-linked macro-oligomers constituted by aniline agglomerates and siloxane oligomeric structures. The barrier action is improved by buffer effect on local alkalinization, which is attributed to combination of labile protons in N–H···N associates with OH^- ions produced near cathodic particles. The effect of Al secondary phases on the protection capability of hybrid PAnSi films in a given local aggressive environment is manifested also. The dissolution of Mg_2Si phase on the AA5083 surface favors Mg-rich PAnSi/AA5083 interface acting as oxygen barrier. Conversely, Zn- and Cu-aniline galvanic couplings are responsible for the outstanding corrosion inhibition of AA7075 and AA2024, respectively, by PAnSi films. Overall results demonstrate the validity of combining silanes and monomers of conducting polymers at a molecular level aimed at obtaining a primer system with synergistic barrier and active actions, which constitutes a promising alternative for chromium-free conversion coatings.

Acknowledgement

The authors are grateful to Dr. M.C. Sala, DiSMAB-Sezione di Chimica Organica "A. Marchesini", for doing the RAIR spectra.

Appendix A. Supplementary data

Supplementary data associated with this article can be found, in the online version, at http://dx.doi.org/10.1016/j.corsci.2012.05.028.

References

[1] D.E. Tallman, G.P. Bierwagen, Corrosion protection using conducting polymers, in: T.A. Skotheim, J.R. Reynolds (Eds.), Handbook of Conducting Polymers, CRC Press, Taylor & Francis Group, New York, 2007, pp. 15/1–15/53.
[2] M. Rohwerder, Conducting polymers for corrosion protection: a review, Int. J. Mater. Res. 100 (2009) 1331–1342.
[3] A.J. Epstein, J.O. Smallfield, H. Guan, M. Fahlman, Corrosion protection of aluminum and aluminum alloys by polyanilines: a potentiodynamic and photoelectron spectroscopy study, Synth. Met. 102 (1999) 1374–1376.
[4] S.F. Cogan, M.D. Gilbert, G.L. Holleck, J. Ehrlich, M.H. Jillson, Galvanic coupling of doped polyaniline and aluminum alloy 2024–T3, J. Electrochem. Soc. 147 (2000) 2143–2147.
[5] J. He, D.E. Tallman, G.P. Bierwagen, Conjugated polymers for corrosion control: scanning vibrating electrode studies of polypyrrole-aluminum alloy interactions, J. Electrochem. Soc. 151 (2004) B644–B651.

[6] L. Cecchetto, D. Delabouglise, J.P. Petit, On the mechanism of the anodic protection of aluminium alloy AA5182 by emeraldine base coatings. Evidences of a galvanic coupling, Electrochim. Acta 52 (2007) 3485–3492;
(b) L. Cecchetto, R. Ambat, A.J. Davenport, D. Delabouglise, J.-P. Petit, O. Neel, Emeraldine base as corrosion protective layer on aluminium alloy AA5182, effect of the surface microstructure, Corros. Sci. 49 (2007) 818–829.
[7] M.C. Yan, D.E. Tallman, G.P. Bierwagen, Role of oxygen in the galvanic interaction between polypyrrole and aluminum alloy, Electrochim. Acta 54 (2008) 220–227.
[8] M. Rohwerder, L.M. Duc, A. Michalik, In situ investigation of corrosion localized at the buried interface between metal and conducting polymer based composite coatings, Electrochim. Acta 54 (2009) 6075–6081.
[9] M.C. Yan, D.E. Tallman, S.C. Rasmussen, G.P. Bierwagen, Corrosion control coatings for aluminum alloys based on neutral and n-doped conjugated polymers, J. Electrochem. Soc. 156 (2009) C360–C366.
[10] M. Rohwerder, S. Isik-Uppenkamp, C.A. Amarnath, Application of the Kelvin Probe method for screening the interfacial reactivity of conducting polymer based coatings for corrosion protection, Electrochim. Acta 56 (2011) 1889–1893.
[11] (a) M. Rizzi, M. Trueba, S.P. Trasatti, Polypyrrole films on Al alloys: The role of structural changes on protection performance, Synth. Met. 161 (2011) 23–31;
(b) E. Volpi, M. Trueba, S.P. Trasatti, Electrochemical investigation of conformational rearrangements of polypyrrole deposited on Al alloys, Prog. Org. Coat. 74 (2012) 376–384.
[12] G.L. Chen, D.E. Tallman, G.P. Bierwagen, Unusual microstructures formed during the mediated electrodeposition of polypyrrole on Al 2024–T3 at low current densities, J. Solid State Electrochem. 8 (2004) 505–510.
[13] (a) N.C.T. Martins, T. Moura eSilva, M.F. Montemor, J.C.S. Fernandes, M.G.S. Ferreira, Electrodeposition and characterization of polypyrrole films on aluminium alloy 6061-T6, Electrochim. Acta 53 (2008) 4754–4763;
(b) N.C.T. Martins, T. Moura eSilva, M.F. Montemor, J.C.S. Fernandes, M.G.S. Ferreira, Polyaniline coatings on aluminium alloy 6061-T6: Electrosynthesis and characterization, Electrochim. Acta 55 (2010) 3580–3588.
[14] K. Kamaraj, S. Sathiyanarayanan, G. Venkatachari, Electropolymerised polyaniline films on AA 7075 alloy and its corrosion protection performance, Prog. Org. Coat. 64 (2009) 67–73.
[15] K.R.L. Castagno, D.S. Azambuja, V. Dalmoro, Polypyrrole electropolymerized on aluminum alloy 1100 doped with oxalate and tungstate anions, J. Appl. Electrochem. 39 (2009) 93–100.
[16] M. Kendig, M. Hon, Environmentally triggered release of oxygen-reduction inhibitors from inherently conducting polymers, Corrosion 60 (2004) 1024–1030.
[17] M. Rohwerder, A. Michalik, Conducting polymers for corrosion protection: what makes the difference between failure and success?, Electrochim Acta 53 (2007) 1300–1313.
[18] (a) J.M. Gustavsson, P.C. Innis, J. He, G.G. Wallace, D.E. Tallman, Processable polyaniline-HCSA/poly(vinyl acetate-co-butyl acrylate) corrosion protection coatings for aluminium alloy 2024–T3: A SVET and Raman study, Electrochim. Acta 54 (2009) 1483–1490;
(b) M. Shabani-Nooshabadi, S.M. Ghoreishi, M. Behpour, Direct electrosynthesis of polyaniline–montmorrilonite nanocomposite coatings on aluminum alloy 3004 and their corrosion protection performance, Corros. Sci. 53 (2011) 3035–3042;
(c) G.-S. Goncalves, A.F. Baldissera, L.F. Rodrigues, E.M.A. Martini, C.A. Ferreira, Alkyd coatings containing polyanilines for corrosion protection of mild steel, Synth. Met. 161 (2011) 313–323;
(d) E. Akbarinezhad, M. Ebrahimi, F. Sharif, M.M. Attar, H.R. Faridi, Synthesis and evaluating corrosion protection effects of emeraldine base PAni/clay nanocomposite as a barrier pigment in zinc-rich ethyl silicate primer, Prog. Org. Coat. 70 (2011) 39–44.
[19] (a) E.C. Gomes, M.A.S. Oliveira, Corrosion protection by multilayer coating using layer-by-layer technique, Surf. Coat. Technol. 205 (2011) 2857–2864;
(b) N.B. Panah, I. Danaee, Study of the anticorrosive properties of polypyrrole/polyaniline bilayer via electrochemical techniques, Prog. Org. Coat. 68 (2010) 214–218;
(c) A.L. Correa-Borroel, S. Gutierrez, E. Arce, R. Cabrera-Sierra, P. Herrasti, Organosilanes and polypyrrole as anticorrosive treatment of aluminium 2024, J. Appl. Electrochem. 39 (2009) 2385–2395.
[20] (a) H. Bhandari, R. Srivastav, V. Choudhary, S.K. Dhawan, Enhancement of corrosion protection efficiency of iron by poly(aniline-co-amino-naphthol-sulphonic acid) nanowires coating in highly acidic medium, Thin Solid Films 519 (2010) 1031–1039;
(b) K. Kamaraj, V. Karpakam, S. Sathiyanarayanan, G. Venkatachari, Electrosysnthesis of poly(aniline-co-m-amino benzoic acid) for corrosion protection of steel, Mater. Chem. Phys. 122 (2010) 123–128.
[21] (a) A. Yagan, N.O. Pekmez, A. Yildiz, Electrochemical synthesis of poly(N-methylaniline) on an iron electrode and its corrosion performance, Electrochim. Acta 53 (2008) 5242–5251;
(b) G. Alvial Moraga, G. Goulart Silva, T. Matencio, R. Magalhaes Paniago, Poly(2,5-dimethoxy aniline)/fluoropolymer blend coatings to corrosion inhibition on stainless steel, Synth. Met. 156 (2006) 1036–1042;
(c) K. Shah, J. Iroh, Electrochemical synthesis and corrosion behavior of poly(N-ethyl aniline) coatings on Al-2024 alloy, Synth. Met. 132 (2002) 35–41;
(d) D. Sazou, Electrodeposition of ring-substituted polyanilines on Fe surfaces from aqueous oxalic acid solutions and corrosion protection of Fe, Synth. Met. 118 (2001) 133–147;
(e) S. Sathiyanarayanan, S.K. Dhawan, D.C. Trivedi, K. Balakrishnan, Soluble conducting polyethoxyaniline as an inhibitor for iron in HCl, Corros. Sci. 33 (1992) 1831–1841.
[22] E. Jaehne, S. Oberoi, H.-J.P. Adler, Ultra thin layers as new concepts for corrosion inhibition and adhesion promotion, Prog. Org. Coat. 61 (2008) 211–223.
[23] (a) M. Trueba, S.P. Trasatti, Pyrrole-based silane primer for corrosion protection of commercial Al alloys Part I: Synthesis and spectroscopic characterization, Prog. Org. Coat. 66 (2009) 254–264;
(b) M. Trueba, S.P. Trasatti, Pyrrole-based silane primer for corrosion protection of commercial Al alloys. Part II: Corrosion performance in neutral NaCl solution, Prog. Org. Coat. 66 (2009) 265–275.
[24] D.O. Flamini, M. Trueba, S.P. Trasatti, Aniline-based silane as a primer for corrosion inhibition of aluminium, Prog. Org. Coat. 74 (2012) 302–310.
[25] R. Akid, M. Gobara, H. Wang, Corrosion protection performance of novel hybrid polyaniline/sol–gel coatings on an aluminium 2024 alloy in neutral, alkaline and acidic solutions, Electrochim. Acta 56 (2011) 2483–2492.
[26] P. Campestrini, E.P.M. van Westing, A. Hovestad, J.H.W. de Wit, Investigation of the chromate conversion coating on Alclad 2024 aluminium alloy: effect of the pH of the chromate bath, Electrochim. Acta 47 (2002) 1097–1113.
[27] W.J. van Ooij, D. Zhu, V. Palanivel, J.A. Lamar, M. Stacy, Overview: the potential of silanes for chromate replacement in metal finishing industries, Silicon Chem. 3 (2006) 11–30.
[28] I. De Graeve, J. Vereecken, A. Franquet, T. Van Schaftinghen, H. Terryn, Silane coating of metal substrates: Complementary use of electrochemical, optical and thermal analysis for the evaluation of film properties, Prog. Org. Coat. 59 (2007) 224–229.
[29] M. Trueba, S.P. Trasatti, Study of Al alloy corrosion in neutral NaCl by the pitting scan technique, Mater. Chem. Phys. 121 (2010) 523–533.
[30] Standard Practice for Laboratory Immersion Corrosion Testing of Metals; ASTM G31–72, 1999, US.
[31] C.-G. Wu, J.-Y. Chen, Chemical deposition of ordered conducting polyaniline film via molecular self-assembly, Chem. Mater. 9 (1997) 399–402.
[32] (a) M.-I. Boyer, S. Quillard, E. Rebourt, G. Louarn, J.P. Buisson, A. Monkman, S. Lefrant, Vibrational analysis of polyaniline: a model compound approach, J. Phys. Chem. B 102 (1998) 7382–7392;
(b) M.-I. Boyer, S. Quillard, G. Louarn, G. Froyer, S. Lefrant, Vibrational study of the FeCl3-doped dimer of polyaniline; a good model compound of emeraldine salt, J. Phys. Chem. B 104 (2000) 8952–8961.
[33] R. Murugesan, E. Subramanian, Metal oxalate complexes as novel inorganic dopants: studies on their effect on conducting polyaniline, Bull. Mater. Sci. 25 (2002) 613–618.
[34] K. Cory Schomburg, R.L. MacCarley, Surface-confined monomers on electrode surfaces. 11. Electrochemical and infrared spectroscopic characteristics of aniline-terminated alkanethiol monolayers on Au electrochemically treated in nonaqueous media, Langmuir 17 (2001) 1993–1998.
[35] T. Lindfors, A. Ivaska, Potentiometric and UV–vis. characterization of N-substituted polyanilines, J. Electroanal. Chem. 535 (2002) 65–74.
[36] C. Ruan, Z. Yang, M.T. Rodgers, Influence of the d orbital occupation on the nature and strength of copper cation–π interactions: threshold collision-induced dissociation and theoretical studies, Phys. Chem. Chem. Phys. 9 (2007) 5902–5918.
[37] M.L. Kantam, M. Roy, S. Roy, B. Sreedhar, R. Lal De, Polyaniline supported CuI: an efficient catalyst for C-N bond formation by N-arylation of N(H)-heterocycles and benzyl amines with aryl halides and arylboronic acids, and aza-Michael reactions of amines with activated alkenes, Catal. Commun. 9 (2008) 2226–2230.
[38] P. Rannou, D. Rouchon, Y.F. Nicolau, M. Nechtschein, A. Ermolieff, Chemical degradation of aged CSA-protonated PANI films analyzed by XPS, Synth. Met. 101 (1999) 823–824.
[39] Y. Liu, M.J. O'Keefe, A. Beyaz, T.P. Schuman, Synthesis and characterization of aluminum–polyaniline thin films and membranes, Surf. Interface Anal. 37 (2005) 782–791.
[40] C. Deslouis, T. El Moustafid, M.M. Mussiani, M.E. Orazem, V. Provost, B. Tribollet, Effect of cations on the diffusivity of the charge carriers in polyaniline membranes, Electrochim. Acta 44 (1999) 2087–2093.
[41] N. Birbilis, R.G. Buchheit, Electrochemical characteristics of intermetallic phases in aluminum alloys. An experimental survey and discussion, J. Electrochem. Soc. 152 (2005) B140–B150.
[42] P. Leblanc, G.S. Frankel, A study of corrosion and pitting initiation of AA2024-T3 using atomic force microscopy, J. Electrochem. Soc. 149 (2002) B239–B247.
[43] G.L. Gutsev, C.W. Bauschlicher Jr., Chemical bonding, electron affinity, and ionization energies of the homonuclear 3d metal dimers, J. Phys. Chem. A 107 (2003) 4755–4767.
[44] K.A. Yasakau, M.L. Zheludkevich, S.V. Lamaka, M.G.S. Ferreira, Role of intermetallic particles in localized corrosion of AA5083, Electrochim. Acta 52 (2007) 7651–7659.
[45] L.T. Sein Jr., Y. Wei, S.A. Jansen, Synth. Met. 143 (2004) 1–12.
[46] V. Palanivel, Y. Huang, W.J. van Ooij, Effects of addition of corrosion inhibitors to silane films on the performance of AA2024-T3 in a 0.5M NaCl solution, Prog. Org. Coat. 53 (2005) 153–168.
[47] S.V. Lamaka, M.L. Zheludkevich, K.A. Yasakau, M.F. Montemor, M.G.S. Ferreira, High effective organic corrosion inhibitors for 2024 aluminium alloy, Electrochim. Acta 52 (2007) 7231–7247.
[48] T.G. Harvey, S.G. Hardin, A.E. Hughes, T.H. Muster, P.A. White, T.A. Markley, P.A. Corrigan, J. Mardel, S.J. Garcia, J.M.C. Mol, A.M. Glenn, The effect of

inhibitor structure on the corrosion of AA2024 and AA7075, Corros. Sci. 53 (2011) 2184–2190.
[49] Z. SzklarskaSmialowska, Pitting corrosion of aluminum, Corros. Sci. 41 (1999) 1743–1767.
[50] (a) W. Pinc, S. Maddela, M. O'Keefe, W. Fahrenholtz, Formation of subsurface crevices in aluminum alloy 2024–T3 during deposition of cerium-based conversion coatings, Surf. Coat. Technol. 204 (2010) 4095–4100;
(b) S. Joshi, B.L. Treu, M.J. O'Keefe, W.G. Fahrenholtz, Characterization of cerium-based conversion coatings on Al 7075–T6 deposited from chloride and nitrate salt solutions, J. Electrochem. Soc. 158 (2011) C88–C93.
[51] G. Bierwagen, R. Brown, D. Battocchi, S. Hayes, Active metal-based corrosion protective coating systems for aircraft requiring no-chromate pretreatment, Prog. Org. Coat. 68 (2010) 48–61.
[52] A. Michalska, Optimizing the analytical performance and construction of ion-selective electrodes with conducting polymer-based ion-to-electron transducers, Anal. Bioanal. Chem. 384 (2006) 391–406.